High-pressure structural phase transition in indium

K. Takemura
National Institute for Research in Inorganic Materials, Tsukuba, Ibaraki 305, Japan

H. Fujihisa
Institute of Materials Science, University of Tsukuba, Tsukuba, Ibaraki 305, Japan
(Received 18 May 1992; revised manuscript received 14 December 1992)

A pressure-induced structural phase transition of indium has been found at 45 GPa using angle-dispersive powder-x-ray-diffraction techniques. The crystal structure of the high-pressure phase In(II) has been determined to be face-centered orthorhombic, which is stable to at least 93 GPa. In(II) is heavily deformed under uniaxial stress. While the volume change at the transition is very close to zero, the transition is likely to be first-order, judging from the coexistence of the low- and high-pressure phases over a wide range of pressure. The structure of In(II) is related to the low-pressure tetragonal phase through a simple orthorhombic distortion, which is in good accord with the structural trends expected from a previous pseudopotential theory.

I. INTRODUCTION

Indium is known as one of the soft metals, which shows excellent ductility at low temperatures. The softness and ductility are closely related to its elastic properties and crystal structure. Indium crystallizes in a face-centered-tetragonal (fct) structure[1] with an axial ratio c/a of 1.0757 at atmospheric pressure. Recent high-pressure x-ray-diffraction experiments revealed that the c/a ratio increases with pressure, reaching a maximum around 24 GPa, and then decreases with further compression.[2] The change in the tetragonal distortion has been discussed in terms of pseudopotential theory. Independent experimental work by Schulte, Nickolaenko, and Holzapfel, up to 30 GPa, also gave similar results.[3] In the previous study, evidence for a structural phase transition was found at around 45 GPa.[2] In this study we have extended the pressure range to about 100 GPa and succeeded in determining the crystal structure of the high-pressure phase.

The present study fully utilizes the excellent features of the imaging plate (IP) as an x-ray area detector. A subtle change in the peak profiles associated with the phase transition was clearly observed in the integrated diffraction pattern available for the high-quality two-dimensional data taken with the IP. Undesired diffraction peaks from the gasket material were digitally subtracted from the raw diffraction data, making a quantitative comparison of the observed and calculated diffraction profiles possible. Inspection of asymmetric peak profiles revealed the existence of heavy elastic deformation in the high-pressure phase In(II). A preliminary account of the present work has been given elsewhere.[4]

II. EXPERIMENT

Indium powder was pressurized directly in a gasketed-diamond anvil cell (DAC) without the use of a pressure medium. Experiments were carried out on three samples. For the experiment using the highest pressure, we used beveled diamond anvils, which have a center flat of 150 μm diameter, bevel angle of 3°, and a culet diameter of 400 μm. An Udimet 700 gasket was indented to a thickness of 30 μm, and a 50-μm-diam hole was drilled at the center. Pressure was determined by the ruby luminescence method.[5] Indium is soft enough to realize a quasihydrostatic environment in the gasket. For this same reason, indium often causes a blowout of the gasket, making pressure generation extremely difficult. Pressures higher than 60 GPa could only be generated by using beveled diamond anvils having *small* bevel angles in combination with a thin gasket. Angle-dispersive powder-x-ray-diffraction patterns were obtained using synchrotron radiation from the bending magnet on beam lines 3A and 6B at the Photon Factory, National Laboratory for High Energy Physics (KEK). The storage ring was operated under a condition of 2.5 GeV and 300 mA. The white x-ray beam was monochromatized with Si(111) double crystals. The second Si crystal was bent sagittally to focus the beam in the horizontal direction.[6] In the case of beam line 3A, a pair of paraboloidal mirrors was inserted in the beam path, so that the incident beam was also focused in the vertical direction.[7] A 40-μm-diam pinhole collimator was placed in front of the DAC to finally reduce the beam size. The position of the DAC was finely adjusted to the incident x-ray beam with the aid of x-ray direct print paper (Linagraph, Kodak) so that the x-ray beam impinged just on the specimen confined in the gasket hole. The diffraction pattern was recorded on an imaging plate[8] and analyzed following the procedure described in Ref. 9. In brief, the image data of a two-dimensional diffraction pattern were reduced to a diffraction profile by integrating the intensity along each Debye-Scherrer ring. An x-ray energy of either 16.87, 18.00, or 20.00 keV was used. Typical exposure times were 3 h. All the experiments were carried out at room temperature.

 ©1993 The American Physical Society

III. RESULTS

High-pressure powder-x-ray-diffraction experiments have been performed up to 93 GPa. As was noted in the previous experiments,[2] new peaks appeared in the diffraction patterns around 45 GPa. For pressures between 45 and 70 GPa, they grew in intensity. Above 70 GPa, the diffraction patterns showed no change with further increases in pressure. We thus conclude that the transition terminates around 70 GPa and the diffraction patterns taken above this pressure are of the single high-pressure phase. Figure 1 shows the representative diffraction patterns of the low-pressure phase In(I) and the high-pressure phase In(II). At first sight, both patterns look very similar. The differences between (a) and (b) result from the addition of peaks near the 200, 202, and 311 reflections in (b) (see arrows), which are absent in (a), and the changes in relative intensity. All the diffraction peaks of the low-pressure fct phase seem to remain in pattern (b). From this one may think that the low- and high-pressure phases still coexist in (b). However, if one indexes those "remaining" peaks to the fct structure, the maximum discrepancy between the observed and calculated d spacings is considerably large ($\sim 0.7\%$), which again supports our interpretation that pattern (b) is of a single high-pressure phase.

In(II) is thus intimately related to the low-pressure phase through a small lattice distortion. Since the new peaks appeared near the 200, 202, and 311 reflections of fct, one can easily visualize an orthorhombic distortion. Figure 2 compares the observed and calculated diffraction profiles for In(II). Figure 2(a) is the same as that shown in Fig. 1(b), only with the scales of intensity and 2θ expanded. Figure 2(b) shows the diffraction profile calculated for a face-centered-orthorhombic (fco) structure with the lattice constants $a = 3.769 \pm 0.003$ Å, $b = 3.846 \pm 0.003$ Å, and $c = 4.140 \pm 0.004$ Å ($a:b:c = 1:1.020:1.098$). The a, b, and c axes of the fco cell correspond, respectively, to the a, b, and c axes of the low-pressure fct cell. The simplest fco structure can be described by the space group D_{2h}^{23}-$Fmmm$ (No. 69), in which four atoms occupy the $4a$ sites. Table I lists the observed and calculated d spacings and intensities. The d spacings are in good agreement to within $\pm 0.2\%$, but the intensities disagree. One also notes significant discrepancies in peak profiles between Figs. 2(a) and 2(b). We consider the origin of these discrepancies next.

One possibility is the effect of preferred orientation. Since the indium specimen was pressurized directly in the gasket without a pressure medium, some lattice planes may align preferentially along the load axis, which is the same as the direction of the incident x-ray beam in the present diffraction geometry. Diffraction intensities are then modulated by the preferential distribution of the lattice planes. However, the observed diffraction pattern Fig. 2(a) contains more features which cannot be ex-

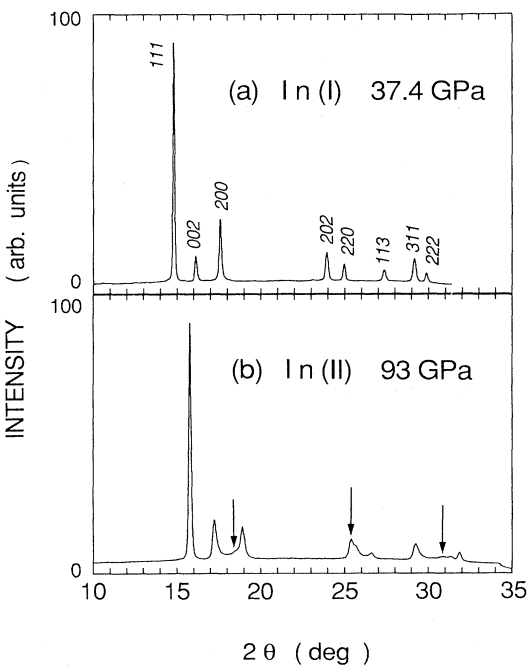

FIG. 1. Powder-x-ray-diffraction patterns of indium under high pressure: (a) the low-pressure phase In(I) at 37.4 ± 0.8 GPa and (b) the high-pressure phase In(II) at 93 ± 5 GPa. Pattern (a) was taken with an x-ray energy of 18.00 keV and (b) with 20.00 keV. The 2θ angles of (a) are converted to those for 20.00 keV for the sake of comparison. Gasket lines are eliminated in (b) as described in Appendix A. The arrows indicate the new diffraction peaks characteristic of In(II).

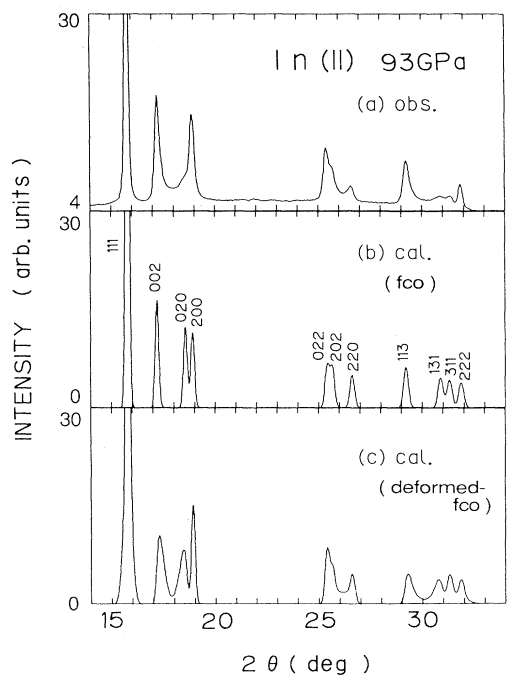

FIG. 2. Observed and calculated diffraction profiles of the high-pressure phase In(II). The x-ray energy is 20.00 keV. (a) Observed at 93 ± 5 GPa [same as Fig. 1(b)]. (b) Calculated for a face-centered-orthorhombic structure. (c) Calculated for the same orthorhombic structure deformed in the $[01\bar{1}]$ direction. See Appendix B for the details of the simulation.

TABLE I. Observed and calculated d spacings and diffraction intensities for In(II) at 93±5 GPa. The lattice parameters for the fco cell are $a=3.769$ Å, $b=3.846$ Å, and $c=4.140$ Å. The calculated diffraction intensities include the absorption corrections.

d_{obs} (Å)	I_{obs}	hkl	d_{cal} (Å)	I_{cal}
2.258	100	111	2.257	100
2.066	26	002	2.070	19
1.922	9	020	1.923	15
1.885	23	200	1.885	14
1.410	11	022	1.409	9
1.396	11	202	1.394	9
1.347	4	220	1.346	7
1.227	15	113	1.228	10
1.164	4	131	1.165	8
1.147	3	311	1.148	7
1.129	7	222	1.128	6

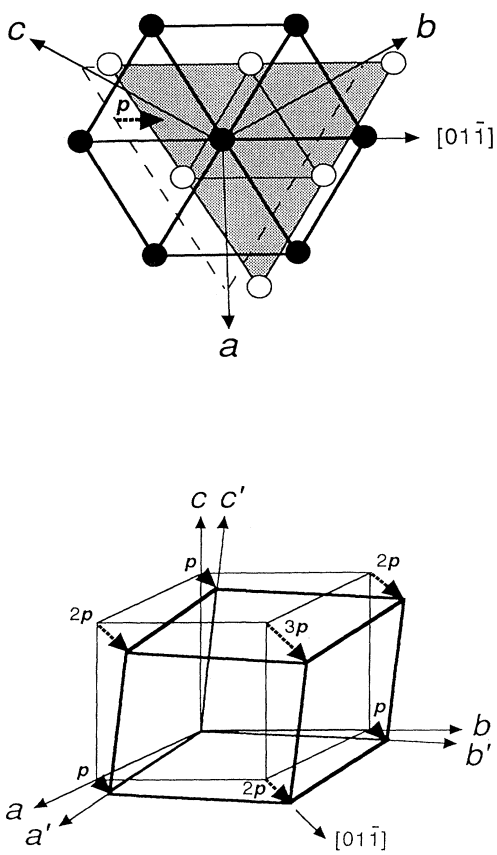

FIG. 3. Model for the deformation in In(II). The top figure shows the [111] projection of the fco lattice. The solid circles represent the atoms in a (111) plane, while the open circles in the adjacent one. Uniaxial stress shifts the atoms in the adjacent (111) plane in the [01$\bar{1}$] direction. **p** denotes the displacement vector. As a result, the unit cell deforms to triclinic as shown by the thick lines in the bottom figure, where **a**, **b**, and **c** are the basis vectors for the fco cell and **a**′, **b**′, and **c**′ for the triclinic one.

plained by the preferred orientation alone: The 002, 220, and 113 reflections have asymmetric peak profiles. More specifically, the "background" between the 002 and 020 reflections is unusually high. These facts indicate that some d spacings have an asymmetric distribution owing probably to anisotropic deformation. Since the 111 reflection remains sharp, the deformation may hardly change the d_{111} interplanar distance. Figure 3 illustrates a model for such a deformation. Here we assume that the orthorhombic (111) planes shift in the [01$\bar{1}$] direction successively. The displacement vector is represented by **p** in the figure. The deformation is assumed to be elastic. The unit-cell volume is kept constant during the deformation. We further assume that the magnitude of the normalized displacement, $\varepsilon=|\mathbf{p}|/(b^2+c^2)^{1/2}$, varies in the specimen according to a Gaussian function. Figure 2(c) shows the diffraction profile thus simulated (see Appendix B for the details of the simulation). The best fit is obtained when the standard deviation of ε is 1.5%. The characteristic features of the observed pattern (a) are now well reproduced in (c), including the high background between the 002 and 020 reflections, which proved to be caused by the overlap of the tails of the two peaks spread in the opposite directions, as well as other asymmetric peak profiles. It should be noted that the deformation in other directions such as [10$\bar{1}$], [1$\bar{1}$0], or [0$\bar{1}$1] does not

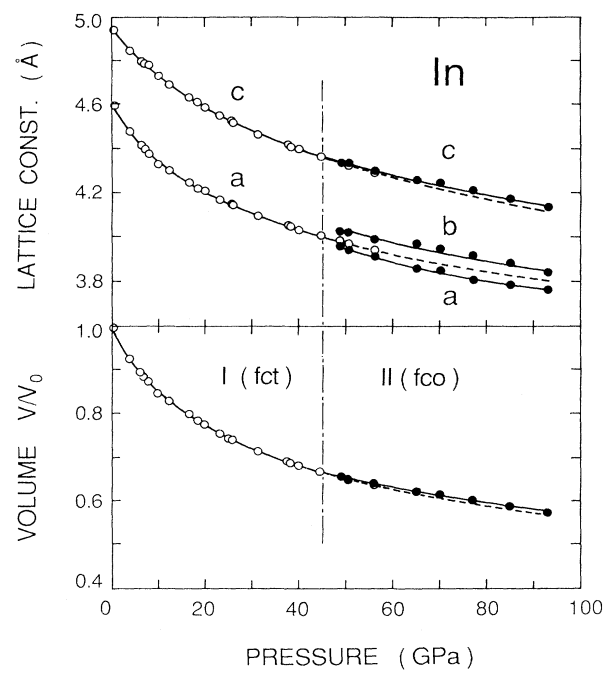

FIG. 4. Change in the lattice constants and the relative volume of indium with pressure. The open and solid circles denote the experimental data for the low-pressure phase I and the high-pressure phase II, respectively. The vertical dot-dashed line shows the onset pressure of the phase transition on increasing pressure. We cannot differentiate between phases I and II in the range 49–56 GPa; thus, the data in this range are shown by assuming both phases. The dashed curves are the extrapolation of the data for phase I to high pressures. The solid curves for phase II are only the guides to the eyes.

reproduce the observed peak profiles, showing that $[01\bar{1}]$ is the preferential displacement direction. No further attempts were made to simulate the observed pattern by including preferred orientation, since it simply increases the number of adjustable parameters in the present case. Further discussions on the nature of the deformation are given in the next section.

It should be emphasized again that the unit cell of In(II) is *undistorted* face-centered orthorhombic, which accidentally deforms under the present experimental conditions. Hence In(II) should be distinguished from the so-called "distorted fcc structure" assigned to the high-pressure phases of Y, La, Pr, and so on.[10] We expect an ideal fco structure for In(II), if it is under a purely hydrostatic condition.

Figure 4 shows the change in the lattice constants and volume of indium with pressure. There was no detectable volume change at the fct-fco transition. The splitting of the tetragonal a axis at the transition, on the other hand, seemed to be discontinuous. The transition was reversible with respect to pressure. The dashed curve in Fig. 4 (bottom panel) shows the extrapolation of the equation of state of the low-pressure phase In(I) with the bulk modulus $B_0=41.8$ GPa and its pressure derivative $B_0'=4.8$.[2] In(II) is stiffer than In(I).

IV. DISCUSSION

The lowering of the crystallographic symmetry of indium at very high pressure can be understood on the basis of the pseudopotential theory by Hafner and Heine.[11] They calculated the real-space interatomic potentials using a simple empty-core pseudopotential. From a characteristic variation of the interatomic potential with electron density and pseudopotential, they proposed a universal phase diagram for the trends in the crystal structures of the elements. Figure 5 reproduces their universal phase diagram for the group-IIIb elements (Fig. 13 of Ref. 11), where each element is plotted according to two parameters: R_s, the electron-density parameter which is proportional to the atomic radius, and R_c/R_s, the ratio of the core radius to the electron-density parameter. Under pressure, R_s decreases, while R_c remains constant. Consequently, the position of an element moves to the upper left in the phase diagram with increasing pressure. For various sets of R_s and R_c/R_s, elastic shear constants are calculated from the interatomic potential. At normal pressure, indium is located in the region where the elastic shear constant C' $[=(C_{11}-C_{12})/2]$ for the fcc structure is negative, resulting in a tetragonal distortion. Since C_{44} for the hcp structure is also negative, hcp-In is likewise unstable. Under pressure, indium moves through the stability region of the fct structure, and approaches the boundary where the shear constant C $(=C_{44})$ becomes negative, leading to a rhombohedral distortion. Beyond the boundary, open-packed structures are expected as in the case of gallium. Although the experimentally identified fco structure cannot be described by the combination of the tetragonal and rhombohedral distortions, the theory explains at least *the instability of fct indium at high pressures.*

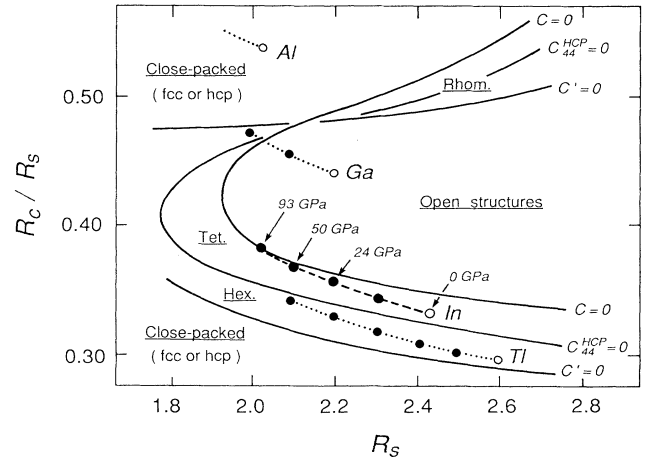

FIG. 5. Universal phase diagram for the group-IIIb elements reproduced from Fig. 13 of Ref. 11. R_s is the electron-density parameter defined by $R_s=R_a z^{-1/3}$, where R_a is the atomic radius (in atomic units) and z the valence. R_c/R_s is the ratio of the core radius R_c to R_s. Pressures indicated for indium are obtained from the pressure-volume relationship of the present work. The data point at 93 GPa is newly added in the present figure. Note that indium approaches the boundary between "Tet. (tetragonal)" and "Open structures" with increasing pressure.

The nature of the deformation in In(II) is not simple. We have assumed elastic deformation in order to explain the asymmetric diffraction profiles. Other deformation models, such as stacking faults or plastic deformation, do not explain the observed diffraction profiles. The stacking faults of the cubic (111) or hexagonal (0001) plane are very common to the close-packed fcc, hcp, or related structures. The effect of stacking faults on the diffraction profile,[12] however, differs from that of the present elastic deformation model in the following two aspects: The stacking faults in the fcc (or fcc-related) structure primarily cause the broadening of the 111 reflection, and the broadening of diffraction peaks is always symmetric. Both effects are not observed in In(II). Our elastic deformation model is not free from problems. The magnitude of the deformation, which is estimated from the simulation of the diffraction profile, is quite large ($\sim 1.5\%$) for elastic deformation. We have no means to check whether the deformation is really elastic, because the recovery process of the deformation cannot be investigated under high pressure. In contrast to In(II), the low-pressure phase In(I) shows no deformation [see Fig. 1(a)], although the stress condition is almost the same. This indicates that the elastic properties of In(II) should be highly anisotropic. Both the fct-fco phase transition and the deformation in In(II) would therefore originate from the elastic anomaly. Further theoretical calculations of elastic moduli for indium with the fco structure may clarify these points.

A question to be answered is whether the In(I) to (II) transition is second order or not. The second-order phase transition shows no hysteresis and has no region of coex-

istence of two phases. In the present experiments, it was difficult to detect the hysteresis within the experimental error. The diffraction patterns of the fct and fco phases were so similar and the pressure inhomogeneity on decreasing pressure was so large that we could not locate the pressure for the backward transition. The fct and fco phases coexisted over a broad pressure range of 45–70 GPa on increasing pressure, judging from the change in the diffraction patterns. This is too large compared with the pressure inhomogeneity ($\sim\pm2$ GPa at 45 GPa), which was determined by the ruby luminescence from different parts of the specimen. Thus the coexistence of the two phases seems to be inherent to the In(I) to (II) transition, suggesting that the transition is likely to be first order. The discontinuity in the lattice constants also indicates the first-order nature of the transition.

A number of high-pressure phases of elemental metals takes the fct (bct) structure. Table II compares the c/a ratios for the high-pressure fct metals. In the cases of the lanthanides (Ce, Sm) and actinide (Th), the stability of the fct structures at high pressures has been discussed in terms of the participation of the f electrons in the bonding.[18,19] On the other hand, the simple metals (In, Ga, and metallic iodine), which have no f electrons, also take the fct structures with c/a ratios identical to those of fct-Ce, Sm, and Th [$(c/a)_{\rm fct}\sim1.08-1.25$]. Skriver argued that there is no correlation between the stability of the fct structure and the $4f$ states in the case of Ce.[20] From the comparison of the c/a ratios, we propose that the fct structures would be stabilized simply by the lowering in the total energy through a lattice distortion as in the present case of indium, but not necessarily by the f bonding. The f bonding should be characterized rather by the short bond length and the low crystallographic symmetry as in the α-U structure.[21] In this regard, the fct to fco phase transition of indium is suggestive as a post-fct transition for these fct metals at ultrahigh pressures.

In summary, we have confirmed the structural phase transition of indium at 45 GPa and at room temperature using high-pressure powder-x-ray-diffraction techniques. The high-pressure phase In(II) is stable to at least 93 GPa. The crystal structure of In(II) has been determined to be face-centered orthorhombic, which is obtained by a simple orthorhombic distortion of the low-pressure tetragonal phase. Peak profiles of In(II) are unusually asymmetric, suggestive of heavy deformation under uniaxial stress. From the simulation of the diffraction profile for the deformed fco structure, we propose that (i) the (111) planes shift in the $[01\bar{1}]$ direction preferentially, (ii) the deformation would be elastic although its magnitude is fairly large ($\sim1.5\%$), and (iii) the elastic properties of In(II) should be highly anisotropic. The instability of the fct structure for indium at high pressures is in good accord with a pseudopotential theory for the structural phase stability of the group-IIIb elements. The volume change at the transition is very close to zero, but the transition is likely to be first order, judging from the discontinuity in the lattice constants and the large region of coexistence of both phases. From a comparison of the c/a ratios of the high-pressure fct metals, we propose that the fct structures would be stabilized commonly by the lowering in the total energy through a lattice distortion.

TABLE II. High-pressure elemental metals with fct (bct) structure. Those having somewhat different c/a ratios, such as Sn [$(c/a)_{\rm fct}=0.65$ at 15 GPa] and Hg [$(c/a)_{\rm fct}=0.52$ at 5 GPa], are omitted in the table (Ref. 13). The c/a ratios for the bct structures, which are obtained by multiplying $\sqrt{2}$ by $(c/a)_{\rm fct}$, are also shown for comparison.

Element	$(c/a)_{\rm fct}$	$(c/a)_{\rm bct}$	P (GPa)	Ref.
In	1.08–1.09	1.53–1.54	0–45	2
Ga	1.12	1.58	2.8	14
I	1.12–1.19	1.58–1.68	42–55	15
Ce	1.16–1.21	1.64–1.71	14–46	16
Sm	1.25	1.77	189	17
Th	1.10–1.17	1.56–1.65	100–300	18

ACKNOWLEDGMENTS

The authors are grateful to Dr. S. Sasaki and Dr. T. Mori for their help in the experiments on the beam line 3A of the Photon Factory. They also thank Dr. O. Shimomura for valuable discussions and critical reading of the manuscript. The present work has been done under Proposal No. 91-091 of the Photon Factory.

APPENDIX A: ELIMINATION OF THE GASKET LINES

Figure 6(a) shows the raw diffraction pattern of In(II) taken at 93±5 GPa. The diffraction lines of the gasket

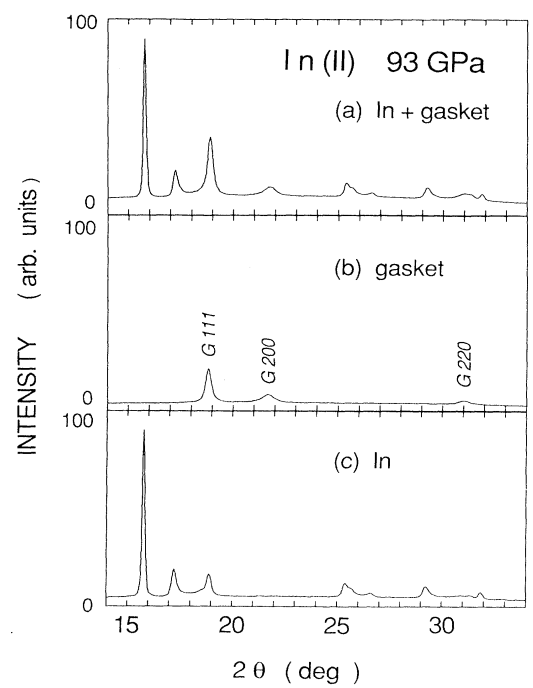

FIG. 6. Diffraction pattern of In(II) at 93±5 GPa taken with an x-ray energy of 20.00 keV. The raw pattern (a) is contaminated with the diffraction lines of the gasket. In order to eliminate them, the diffraction pattern only of the gasket is taken in the vicinity of the specimen [(b)], and subtracted from (a) after several corrections, yielding pattern (c).

overlapped with those of indium. The gasket lines, however, were successfully eliminated as follows. We took the diffraction pattern of the gasket in the vicinity of indium by changing the position of the DAC by about 50 μm [(b)]. After the corrections for the exposure time, intensity of the incident x-ray beam, and slight shift in the peak positions ($\sim 0.06°$ in 2θ), pattern (b) was digitally subtracted from (a). The obtained pattern (c), which is identical to those shown in Figs. 1(b) and 2(a), consists only of indium. It was essential to use the diffraction pattern of the gasket under exactly the same experimental conditions as the specimen, since the positions, profiles, and intensities of the gasket lines were very sensitive to any change in the uniaxial stress.

APPENDIX B: SIMULATION OF THE DIFFRACTION PATTERN FOR THE DEFORMED fco STRUCTURE

The pattern [Fig. 2(c)] was simulated as follows. If the atoms in every (111) plane of the fco cell shift in the $[01\bar{1}]$ direction successively, the unit cell becomes triclinic (see Fig. 3). The basis vectors $\mathbf{a}'$, $\mathbf{b}'$, and $\mathbf{c}'$ for this conventional triclinic cell can be written with the basis vectors $\mathbf{a}$, $\mathbf{b}$, and $\mathbf{c}$ for the undeformed fco cell and the displacement vector $\mathbf{p}$ as

$$\mathbf{a}'=\mathbf{a}+\mathbf{p} ,$$

$$\mathbf{b}'=\mathbf{b}+\mathbf{p} ,$$

$$\mathbf{c}'=\mathbf{c}+\mathbf{p} ,$$

$$\mathbf{p}=(0,\varepsilon b,-\varepsilon c) ,$$

where ε represents the magnitude of the displacement vector normalized with the magnitude of the $[01\bar{1}]$ lattice vector:

$$\varepsilon=|\mathbf{p}|/(b^2+c^2)^{1/2} .$$

We assume that ε distributes according to a Gaussian function

$$F(\varepsilon)=A\exp[-\varepsilon^2/(2\sigma^2)] ,$$

where $F(\varepsilon)$ denotes the probability, A the scale factor, and σ the standard deviation. If we express the diffraction profile for given ε by $P(\varepsilon)$, then the final pattern P_f is obtained by summing up $P(\varepsilon)$ weighted by $F(\varepsilon)$ as

$$P_f=\sum_{\varepsilon=0}^{\infty} F(\varepsilon)P(\varepsilon) .$$

We have optimized P_f by changing σ so that it reproduces the observed pattern [Fig. 2(a)]. The best fit was obtained when $\sigma=0.015$.

[1]The correct unit cell for indium is body-centered tetragonal (bct) belonging to the space group D_{4h}^{17}-$I\,4/mmm$ (No. 139). However, since the deviation from fcc is small ($\sim 7\%$), we prefer to use a face-centered-tetragonal (fct) cell. The fct cell is easy to compare with the fcc as well as with the presently found fco structures.

[2]K. Takemura, Phys. Rev. B **44**, 545 (1991).

[3]O. Schulte, A. Nikolaenko, and W. B. Holzapfel, High Press. Res. **6**, 169 (1991).

[4]K. Takemura, in *Recent Trends in High Pressure Research,* edited by A. K. Singh (Oxford & IBH, New Delhi, 1992), pp. 187–189.

[5]H. K. Mao, P. M. Bell, J. W. Shaner, and D. J. Steinberg, J. Appl. Phys. **49**, 3276 (1978).

[6]A. Koyama, M. Nomura, H. Kawata, T. Iwazumi, M. Sato, and T. Matsushita, Rev. Sci. Intrum. **63**, 916 (1992).

[7]S. Sasaki, T. Mori, A. Mikuni, H. Iwasaki, K. Kawasaki, Y. Takagi, and K. Nose, Rev. Sci. Instrum. **63**, 1047 (1992).

[8]Y. Amemiya, Y. Satow, T. Matsushita, J. Chikawa, K. Wakabayashi, and J. Miyahara, Top. Curr. Chem. **147**, 121 (1988).

[9]O. Shimomura, K. Takemura, H. Fujihisa, Y. Fujii, Y. Ohishi, T. Kikegawa, Y. Amemiya, and T. Matsushita, Rev. Sci. Instrum. **63**, 967 (1992).

[10]Y. K. Vohra, V. Vijayakumar, B. K. Godwal, and S. K. Sikka, Phys. Rev. B **30**, 6205 (1984); S. K. Sikka and V. Vijayakumar, Physica B **144**, 23 (1986).

[11]J. Hafner and V. Heine, J. Phys. F **13**, 2479 (1983).

[12]R. Berliner and S. A. Werner, Phys. Rev. B **34**, 3586 (1986).

[13]For compilations of the high-pressure structural data of the elements, see, for example, D. A. Young, *Phase Diagrams of the Elements* (University of California Press, Berkeley, 1991); L. G. Liu and W. A. Bassett, *Elements, Oxides, Silicates: High-Pressure Phases with Implications for the Earth's Interior* (Oxford University Press, New York, 1986); J. Donohue, *The Structures of the Elements* (Wiley, New York, 1974).

[14]L. Bosio, J. Chem. Phys. **68**, 1221 (1978).

[15]Y. Fujii, K. Hase, Y. Ohishi, N. Hamaya, and A. Onodera, Solid State Commun. **59**, 85 (1986); K. Hase, thesis, Osaka University, 1988.

[16]J. S. Olsen, L. Gerward, U. Benedict, and J. P. Itié, Physica B **133**, 129 (1985).

[17]Y. K. Vohra, J. Akella, S. Weir, and G. S. Smith, Phys. Lett. A **158**, 89 (1991).

[18]Y. K. Vohra and J. Akella, Phys. Rev. Lett. **67**, 3563 (1991).

[19]J. M. Wills, O. Eriksson, and A. M. Boring, Phys. Rev. Lett. **67**, 2215 (1991); O. Eriksson, P. Söderlind, and J. M. Wills, Phys. Rev. B **45**, 12 588 (1992); R. S. Rao, B. K. Godwal, and S. K. Sikka, *ibid.* **46**, 5780 (1992).

[20]H. L. Skriver, Phys. Rev. B **31**, 1909 (1985).

[21]C. W. Jacob and B. E. Warren, J. Am. Chem. Soc. **59**, 2588 (1937); R. B. Roof, R. G. Haire, D. Schiferl, L. A. Schwalbe, E. A. Kmetko, and J. L. Smith, Science **207**, 1353 (1980).